Journal of Biomedical Optics

SPIEDigitalLibrary.org/jbo

Detection of localized inclusions of gold nanoparticles in Intralipid-1% by point-radiance spectroscopy

Serge Grabtchak
Tyler J. Palmer
William M. Whelan

SPIE

Detection of localized inclusions of gold nanoparticles in Intralipid-1% by point-radiance spectroscopy

Serge Grabtchak,[a,b] Tyler J. Palmer,[a] and William M. Whelan[a,c]
[a]University of Prince Edward Island, Department of Physics, Charlottetown, Prince Edward Island Canada C1A 4P3
[b]Dalhousie University, Department of Electrical and Computer Engineering, Halifax, Nova Scotia Canada B3J 1Z1
[c]Atlantic Veterinary College, Department of Biomedical Sciences, Charlottetown, Prince Edward Island Canada C1A 4P3

Abstract. Interstitial fiber-optic–based approaches used in both diagnostic and therapeutic applications rely on localized light-tissue interactions. We present an optical technique to identify spectrally and spatially specific exogenous chromophores in highly scattering turbid media. Point radiance spectroscopy is based on directional light collection at a single point with a side-firing fiber that can be rotated up to 360 deg. A side firing fiber accepts light within a well-defined, solid angle, thus potentially providing an improved spatial resolution. Measurements were performed using an 800-μm diameter isotropic spherical diffuser coupled to a halogen light source and a 600 μm, ~43 deg cleaved fiber (i.e., radiance detector). The background liquid-based scattering phantom was fabricated using 1% Intralipid. Light was collected with 1 deg increments through 360 deg-segment. Gold nanoparticles , placed into a 3.5-mm diameter capillary tube were used as localized scatterers and absorbers introduced into the liquid phantom both on- and off-axis between source and detector. The localized optical inhomogeneity was detectable as an angular-resolved variation in the radiance polar plots. This technique is being investigated as a potential noninvasive optical modality for prostate cancer monitoring. [DOI: 10.1117/1.3597624]

Keywords: point-radiance spectroscopy; intralipid; gold nanoparticles; plasmonics scattering; absorption; interstitial fiber-optic diagnostics.

Paper 11117PR received Mar. 9, 2011; revised manuscript received Apr. 28, 2011; accepted for publication May 16, 2011; published online Jul. 1, 2011.

1 Introduction

There is a need for optical techniques to monitor tissues during and after therapies such as laser interstitial thermal therapy (LITT)[1–3] and photodynamic therapy (PDT).[4] LITT delivers energy to tissues in a form of light that is absorbed by chromophores and transformed into heat in a very selective and localized way. PDT also relies on localized light delivery. Both techniques require knowledge of spatially-resolved tissue optical properties that affect light propagation and energy deposition. Optical parameters of interest include absorption and scattering properties, chromophore identification, and localization. A detection technique that could monitor changes in optical propagation in real time would be very beneficial for online treatment. Aside from LITT and PDT, a noninvasive or minimally invasive optical modality could provide a convenient solution for routine medical diagnostics of organs and tissues by detecting changes in the optical properties (optical inhomogeneities) produced by certain diseases.

Light is often detected in tissues through interstitial fibers in open or closed catheters. A commonly used probe (known as a fluence probe) has an isotropic diffused sphere attached to the end of the fiber that measures the integrated light collected over a 4π solid angle. Typically, optical properties can be determined by fitting the diffusion theory for light transport in tissue to relative fluence measurements performed at known source detector separations.[4–6] To overcome a problem of nonuniqueness in the optical property recovery, interstitial characterization of tissue optical properties has typically required absolute fluence measurements that can be difficult to obtain accurately.

With the development of directional sensors, alternative characterization and monitoring techniques have emerged.[7–9] A probe that collects light from a cone in one specific direction is known as a radiance detector. The radiance detector can be constructed by attaching a right angle microprism to a multimode optical fiber.[7] Using relative radiance measurements at a single distance and the P3 approximation as an optical model for fitting, Dickey et al.[7] demonstrated the ability to characterize the optical properties of liquid optical phantoms. Chin et al.[8] examined the uniqueness of optical property recovery by radiance detection. An extension of the technique to multiple wavelengths and two detection angles has also been demonstrated.[9] Due to its angular-resolved light collection, the radiance detector can, in principle, provide a spatial resolution of measured optical properties, but this feature has yet to be investigated.

Out of the variety of exogenous chromophores used in biomedical research, gold nanoparticles (Au NPs) deserve special attention. Selectively enhanced interaction with light due to localized plasmon resonances produces scattering and absorption cross-sections that are about 4 to 5 orders of magnitude higher than those of known organic dyes.[10] Au NPs have size-dependent optical properties: their absorption cross-sections increase linearly with particle volume, while their scattering

Address all correspondence to: Serge Grabtchak, University of Prince Edward Island, Department, of Physics, 550 University Avenue, Charlottetown, Prince Edward Island C1A 4P3 Canada. Tel: 902-566-6078; Fax: 902-566-0483; E-mail: sgrabtchak@upei.ca.

1083-3668/2011/16(7)/077003/9/$25.00 © 2011 SPIE

cross-sections scale with the square of the volume.[11] A proper surface functionalization followed by a subsequent specific binding to targeted sites makes Au NPs excellent molecular contrast agents at cellular levels[12] when used with optical imaging modalities. When applied to cancerous tissue imaging, Au NPs serve as a valuable tool for cancer delineation.[13] A therapeutic effect of Au NPs, due to the efficient conversion of absorbed light to locally released heat has also been demonstrated in causing malignant tissue death through protein coagulation.[14] However, one of the challenges in nanoparticle mediated thermal therapy is the inability to visualize particle distribution within tumors.[15] Therefore, both diagnostic and therapeutic applications of Au NPs, when coupled with noninvasive optical modalities, require the ability to identify the chromophore and spatially locate it. When Au NPs are dispersed in highly scattering biological tissues and used as contrast agents for tumor visualization/delineation, depending on the experimental method, either the scattering (in reflectance mode confocal microscopy,[16] optical coherence tomography,[16,17] and diffuse reflectance spectroscopy[18]) or absorption properties[13] can be exploited. Therefore, detecting strong scatterers or strong absorbers (or both) in a highly scattering medium is a topic of particular interest for biomedical optics. This aspect prompted us to select Au NPs that possess both substantial scattering and absorption for the current study.

Intralipid is a soy bean oil emulsion that is frequently used as a background medium for liquid phantoms to mimic optical properties of tissues. Absolute values of optical properties of prostate are scarce and show substantial interorgan and intraorgan variations: 0.1 to 1.6 cm^{-1} for the absorption coefficient and 1.2 to 40 cm^{-1} for the reduced scattering coefficient measured at 732 nm in prostate carcinoma.[4] Intralpid-based phantoms are cost-effective solutions that allow to vary the reduced scattering coefficient in a wide range [from 100 cm^{-1} (Intralipid-10%) to 350 cm^{-1} (Intralipid-30%) at 700 nm][19] that can be adjusted easily to match the corresponding properties of the biological tissues of interest. A relatively small optical absorption of tissues can be accounted by adding controlled concentrations of Naphthol green dye to the Intralipid medium.[9] Optical extinction of Intralipid solutions is due to water absorption and Mie scattering of lipid particles.[19,20] Data on the scattering properties of Intralipid-1% show some spread mainly due to fabrication variations between different brands. Variations in the particle size used in Intralipid fabrication transform to variations of the anisotropy factor.[19] Because the particle size stays constant during dilutions, Intralipid-1% solutions obtained from various stock solutions (i.e., 10%, 20%, etc.) would have different anisotropy factor values and as a result, different values of the reduced scattering coefficient. Even though stock solution information was not always reported, we have attempted to summarize the published data in Fig. 1 where the reduced scattering coefficient versus wavelength is plotted for Intralipid-1%. To create the plot, we took data from Dam et al.,[21] Solonenko et al.,[22] and added data obtained by McGlone et al.,[20] along with other values cited in the article. Data for the reduced scattering coefficient for Intralipid-1% fall within the range of values for the reduced scattering coefficient of the prostate, indicating a suitability of Intralipid-1% as the background phantom medium for prostate-simulated studies.

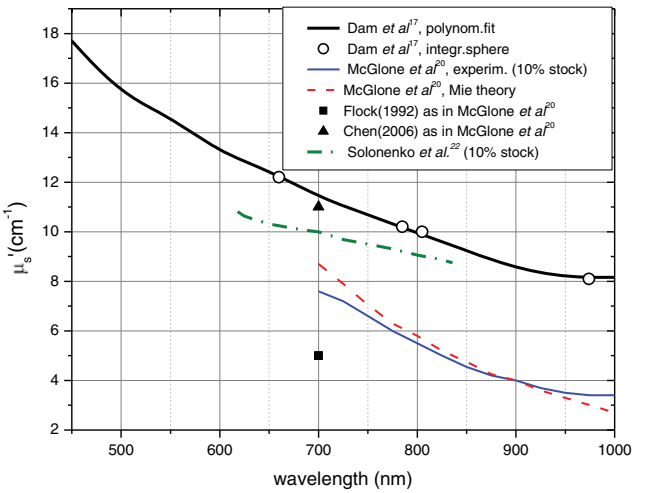

Fig. 1 A compilation of known literature data for the reduced scattering coefficient of Intralipid-1%.

In the present work, we advance the point radiance spectroscopy approach by using commercially available side firing fibers as radiance detectors. Second, we have developed an automated and versatile platform to study the effects of localized Au NP inclusions in a liquid scattering medium on radiance profiles taken over the entire 360 deg range. Third, we have demonstrated features in the radiance profile that provide information on the chromophore's absorption spectrum and angular location.

2 Materials and Methods

2.1 *Point Radiance Spectroscopy Set-up*

Figure 2(a) shows a schematic block-diagram of the experimental setup [Fig. 2(b) presents a view of the fiber positioning stages and the phantom box)]. Light from a tungsten halogen white light source (HL-2000 20 W, Ocean Optics, USA) was coupled to an 850-μm isotropic probe fiber (Medlight, Switzerland) that served as a spherical source [see inset of Fig. 2(b)]. The output power from the tip of the spherical diffuser was measured to be ~3 mW (using a plane detector), hence, the total power coming from the source fiber was estimated to be ~18 mW. The source fiber was positioned in a holder mounted on a *x,y*-translation stage with an additional *z*-axis control micrometer. A 600-μm core side firing fiber cleaved ~43° at the distal end [see inset of Fig. 2(b)] was used as a radiance detector (Polymicro Technologies/Molex, USA). The fiber's numerical aperture (NA) based on a plane-cut tip was 0.24 (specified by the manufacturer). A protective cap (silica) on the fiber end preserved the total internal reflection condition upon immersing the fiber in a liquid. Both source and detector fibers were threaded through 1.1 mm (o.d.) stainless steel tubes. The detector fiber was mounted on a computer-controlled motorized rotation mount (Thorlabs, USA) that allowed complete 360 deg rotation with a 1 deg step. The detector fiber was connected to a computer interfaced spectrometer (USB-4000, Ocean Optics, USA) for signal acquisition in the 400 to 900 nm range. The integration time was 100 ms and four signal averaging was used. The sample (250-nm diameter Au colloid) was held in a 3.5-mm diameter thin walled quartz

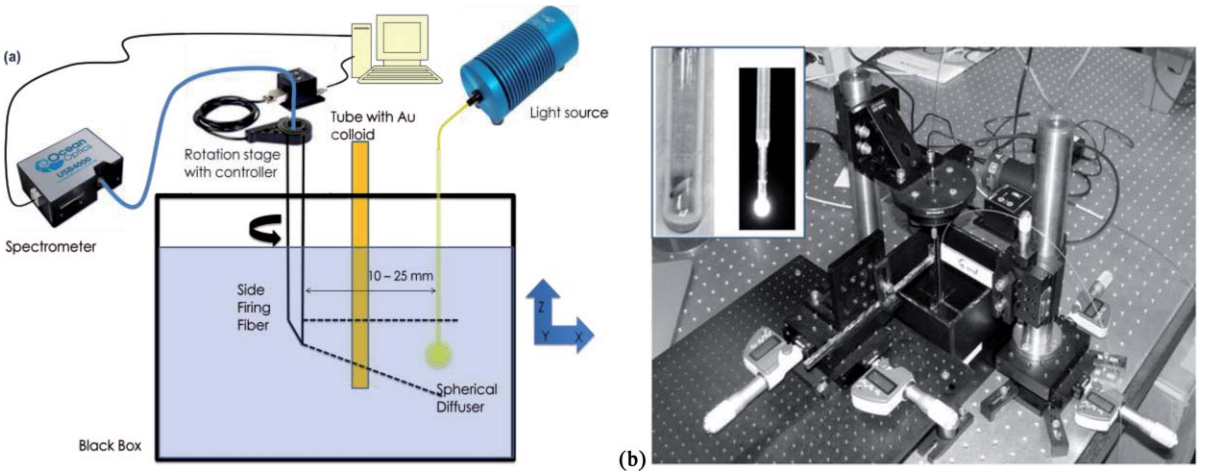

Fig. 2 An experimental set-up for point-radiance measurements in liquid phantoms: (a) schematic, (b) a view of fiber positioning stages, and the phantom box. Inset in (b) a side-firing fiber (radiance detector) and a spherical diffuser (light source).

capillary tube, and the tube position was controlled in the *x,y*-plane by two translation stages. The source, detector, and tube were positioned in the middle of the phantom lucite box (18× 18×18 cm) with blackened walls. Experiments were conducted in air, water, and Intralipid-1%, all at room temperature (21°C).

2.2 *Intralipid Phantom and 250-nm Gold Nanoparticles*

Intralipid-1% was used as the background optical medium and was prepared by a volume dilution of a stock solution of Intralipid-20% (Sigma-Aldrich, Canada) with deionized water. The phantom box was completely filled with ∼1.8 L of Intralipd-1% solution. To focus the study on detection of Au NPs in highly scattering medium, the optical absorption of the Intralipid solution was not modified by adding dyes. We took an incremental approach to targeting the relevant prostate geometry by considering the localized optical inhomogeneities in an infinite medium. While it is relatively difficult to build a three-dimensional (3D) phantom model with easily adjustable optical properties of the background and a placement of localized inhomogeneities which would preserve the ease of the fiber manipulation, liquid phantoms allow an implementation of open access models with two-dimensional (2D) cylindrical symmetry (i.e., in-plane measurements). A localized inhomogeneity for the 2D phantom is approximated by a cylinder. Therefore, we started our study with a "borderless" model in order to focus on the properties of the turbid medium. However, due to the inherent 3D nature of photon scattering, the interaction between photons and the cylinder-shaped inhomogeneity can not be restricted to the in-plane.

Water-based 250-nm diameter Au colloid with a concentration of 3.8×10^8 particle/ml (Ted Pella, USA) was used as the target of optical inhomogeneity. Results of a Mie theory calculation[23] of the extinction, scattering, and absorption efficiencies for a single 250-nm diameter Au particle in water are shown in Fig. 3(a). Optical extinction is the sum of scattering and absorption. The extinction efficiency is defined as the

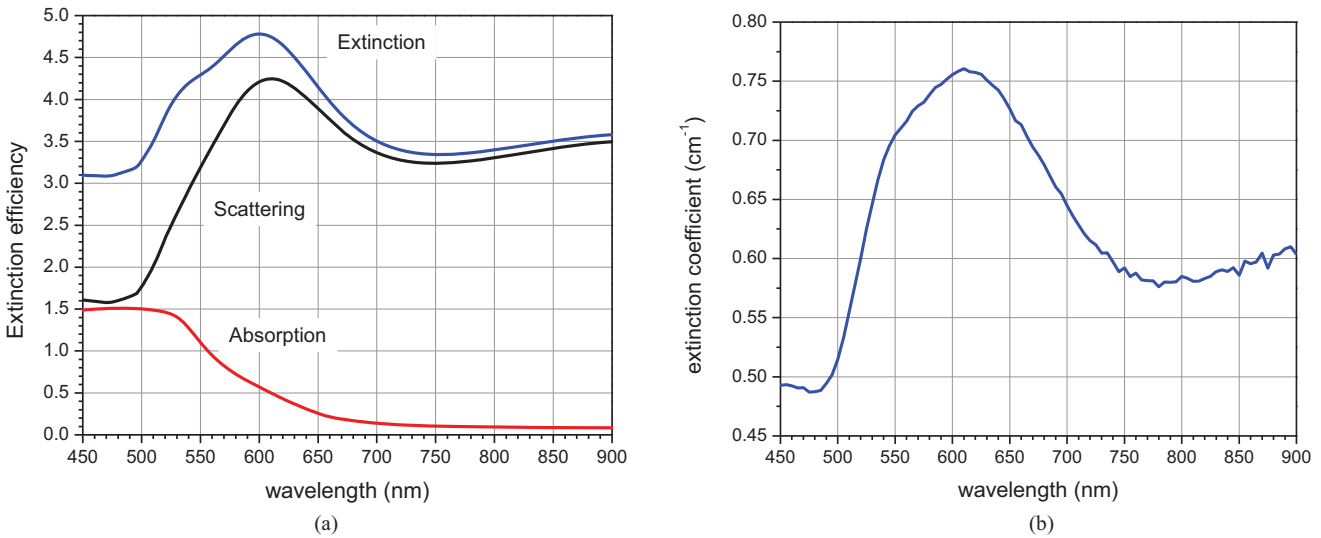

Fig. 3 Optical properties of 250 nm Au particles in water: (a) Mie theory-based calculated extinction, scattering, and absorption efficiencies, and (b) measured extinction coefficient (1 cm cuvette, Cary 50).

extinction cross-section divided by the geometrical cross-section. Large particle size effects are noticeable in the scattering curve where the retardation effect is manifested in the appearance of the quadrupole resonance (~620 nm), in addition to the dipole one (above 900 nm, not seen). The absorption curve undergoes relatively minor changes when compared with particles of smaller sizes. Another size-related effect is also evident—the particle becomes an approximately three times more efficient scatterer than an absorber. The measured extinction (1 cm cuvette, Cary 50) was converted into the extinction coefficient and is shown in Fig. 3(b). Theoretical single particle extinction efficiency (C_{ext}) was converted into the extinction coefficient (μ_{ext}) using the particle density (N) in the Au colloid provided by the manufacturer using the following relation: $\mu_{ext} = N \cdot C_{ext} \cdot \pi r^2$, where r is the radius of the particle. The experimental and theoretical extinction coefficients curves showed agreement within ~10%.

2.3 *Methodology of Measurements*

For each experiment, the source fiber and the radiance detector were positioned at a fixed separation distance, aligned vertically to maximize the signal, and an angular radiance profile was taken by rotating the detector. A set of two radiance profiles was acquired for each source-detector separation, one with the background medium alone (i.e., no sample) and a second with the Au NPs filled capillary tube (i.e., sample). The ratio of two profiles (no-sample/sample) was analyzed and reported. This ratio bears similarity to that normally used in spectroscopy for absorbance (A): $A(\lambda) = \log_{10}[I_0(\lambda)/I_s(\lambda)]$, where I_0 is the incident intensity, I_s is the transmitted intensity with the sample present and λ is the wavelength. Absorbance is replaced with optical extinction when the sample has scattering centers in addition to absorption. To emphasize the difference with traditional spectroscopy (in illumination and collection geometries), we report the ratio $I_I(\lambda)/I_{Au+w}(\lambda)$ as a radiance extinction ratio of Au colloid (containing both Au and water, w) in the Intralipid solution. (Note, that we did not take the logarithm of the ratio). We posit that the ratio of these two radiance profiles should yield information on the spectral and spatial perturbation in the diffuse optical propagation due to the presence of a localized optical inhomogeneity. (In separate experiments, the effect of the quartz capillary tube was found to be negligible.) To separate the contributions from water and gold *per se* in the colloidal solution, an additional measurement was also conducted: water filled tube in Intralipid to produce $I_I(\lambda)/I_w(\lambda)$. It also allowed to compare Au colloid filled tube in Intralipid with water filled tube in Intralipid via $I_w(\lambda)/I_{Au+w}(\lambda)$. The first ratio elucidates the water effect and the second the effect of Au NPs.

One angular profile with selected parameters (360 positions with 1 deg step, 100 ms integration time, 4 averages) was acquired in 10 min. However, our data show that a 1 deg step is excessive and could easily be replaced by a ~4 deg step without a loss of resolution. The signal/noise ratio can also be improved while keeping the total measurement cycle under 10 min.

3 Results and Discussion

3.1 *Side Firing Fiber Performance in Air and Water*

The setup was initially tested in air and water backgrounds. The resulting angular radiance profiles plotted in polar coordinates and normalized to the maximum intensity are shown in Fig. 4 [in air, Fig. 4(a) and in water, Fig. 4(b)]. Detected spectra in air and water are influenced by the output of the white light source, fiber transmission characteristics, and the spectrometer response. However, the shape of the radiance profiles measured at all wavelengths was nearly identical. Hence, a wavelength of 520 nm was selected for comparison purposes. Angular detection of isotropic white light source with a side firing fiber [in air, Fig. 4(a) and water, Fig. 4(b)] produces a narrow lobe in polar coordinates whose width is a convolution of the point-like source with the full acceptance angle of the fiber. Hence, the lobe width is mostly determined by the numerical aperture of the fiber and the refractive index of the medium. The NA of the fiber is linked to the internal critical angle determined by the refractive indexes of the fiber core and fiber cladding and is a constant value: NA = n*sinθ = const where n is the refractive index of the surrounding medium and θ is the half-acceptance angle.[24] However, the NA of the side firing fiber may deviate from the plane-cut fiber due to complex refractions at a curved glass interface which yield two different acceptance angles in two orthogonal planes.[25] When the fiber is immersed into a

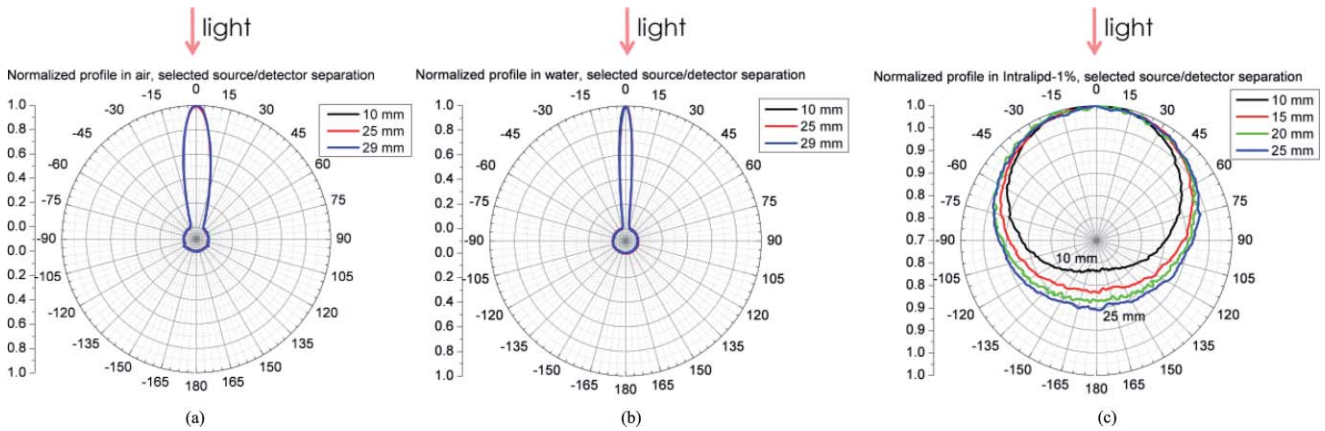

Fig. 4 Normalized to maximum values radiance profiles in (a) air, (b) water, and (c) Intralipid-1% at 520 nm for selected source-detector separations. No tube with chromophore.

medium with $n>1$ the acceptance angle decreases accordingly. Half-angle values extracted from the polar plots, 11 deg (air) and 5 deg (water), are smaller than corresponding values for the plane-cut fiber in air (14 deg) and water (8.3 deg). The values may serve as a first approximation of the true NA. As expected, the shape of radiance profiles in air and in water was preserved at all source-detector separations indicating a constant NA.

3.2 *Gold Nanoparticles in Intralipid Phantom*

Angular radiance profiles in Intralipid-1% normalized to the maximum intensity are shown in Fig. 4(c). In the Intralipid preparations, water may account for up to 99% of the solution, depending on the concentration. Hence, the refractive index of Intralipid is expected to be similar to water. However, the profile measured in Intralipid-1% bears no resemblance to that in water [Fig. 4(b)]. For Intralipd-1%, the radiance profile widens significantly and acquires an off-centered circular-type feature. This is a manifestation of the multiple scattering events and a distribution of photons pathlengths that occur in highly scattering media such as, Intralipid. In order to be detected by the side firing fiber, photons must be approximately one scattering pathlength away from the outer interface of the fiber and inside the solid angle acceptance cone ($\sim$ 10 deg), which for Intralipid is very similar to water.

The profiles measured in Intralipid-1% at various source-detector separations do not preserve the shape as seen in Fig. 4(c). Anisotropy in the profiles observed at all distances is more pronounced at shorter ones. For example, Intralipid-10% has an anisotropy factor g ranging from 0.7 at 400 nm to $\sim$0.4 at 650 nm, indicating a preferential forward scattering.[19] Our experimental radiance profiles agree qualitatively with the results of Monte Carlo simulation[26] and diffusion theory predications.[27] The response of radiance to the increase of the separation between the source and the detector demonstrated a decrease of radiance anisotropy (seen as a relative increase of the backscattered light). This is consistent with Monte Carlo simulations results and is linked to the Henyey–Greenstein distribution that describes the scattering phase function.[26] It follows that a reversal of the photon pathway will occur after multiple successive scattering events rather than from a single deflection at a single scattering event. An increase in the source-detector separation increases the longevity of the photon packet which is accompanied by an increase in the number of photons with path reversal and therefore, contributes to the backscattered signal.[26]

Placing the sample into a background of Intralipid-1% perturbs a distribution of chromophores by introducing a localized optical inhomogeneity. To isolate the spectroscopic signature of the chromophore, we analyzed the ratio of the system response without the sample to the response with the sample at a given detector position. An analogy with data manipulation in typical spectroscopic measurements with a common spectrophotometer is helpful. A sample of interest is usually dissolved in a solvent (frequently, water) and placed in a cuvette surrounded by an outside medium. Because the outside medium is air, no correction is required. Therefore, the effect of the solvent, as well as the spectral profile of the light source and the spectrometer response, is taken into account by proper referencing to the blank (usually, cuvette with water). In our measurements, the surrounding medium is Intralipid and the solvent is water. Therefore, our measurements include an extra step of referencing to the surrounding medium (i.e., Intralipid) in addition to referencing to water.

The first set of translation measurements was conducted by keeping the source-detector separation constant at 12 mm with the detector always facing the source (i.e., no angular rotation) and the Au colloid sample positioned initially mid-way between the source and the detector. This corresponded to a zero offset from the source-detector direction. The sample was then translated orthogonally to the source-detector line with a 0.5 mm increment up to 18 mm from the source-detector direction, acquiring data at every position. Then, an Au colloid sample was replaced by the water sample and the measurements were repeated for the same sample positions. The radiance extinction ratios of Au colloid in Intralipid, $[I_I(\lambda)/I_{Au+w}(\lambda)]$ and Au in Intralipid, $[I_w(\lambda)/I_{Au+w}(\lambda)]$ (shifted vertically for clarity) are shown in Fig. 5 for a 0 mm offset.

The first remarkable feature is that the spectrum of Au NPs from Fig. 5 does not coincide with the extinction spectrum from Fig. 3, but with the absorption that is also shown on the plot. It can be understood in terms of independent scattering approximation.[5,17] Absorption and scattering coefficients of the system (Intralipid with Au NPs) can be considered as a linear combination of the optical properties of the background medium (Intralipid) and exogenous contrast agents (Au NPs). The scattering coefficient of Intralipid-1% can be estimated to be $\sim$64 cm^{-1} from known values of the reduced scattering coefficient ($\sim$16 cm^{-1} at 500 nm from Fig. 1) and the anisotropy factor ($g = 0.75$ at 500 nm for Intralipid-20%).[19] Comparing it with the maximum possible value of the scattering coefficient for Au NPs (0.75 cm^{-1}), it is clear that the total scattering coefficient of the Intralipid-1% with a Au NPs system should be dominated by Intralipid scattering. This is a rather simplistic approach, taken because the exact contribution of scattering and absorption coefficients to the measured radiance ratios is not

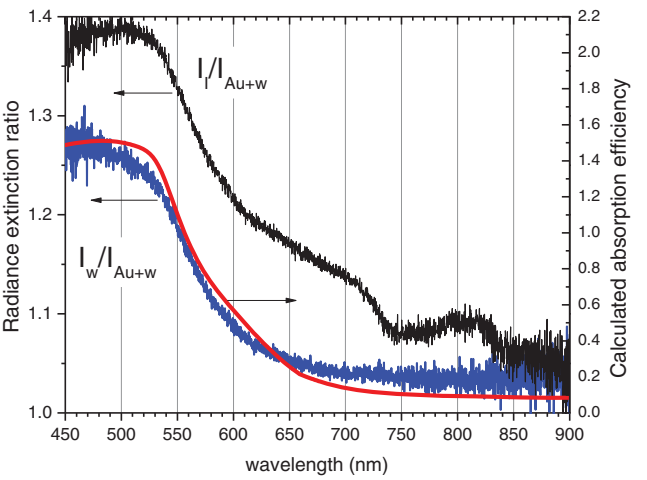

Fig. 5 Individual radiance extinction ratios of Au colloid in Intralipid, (I_I/I_{Au+w}) and Au in Intralipid, (I_w/I_{Au+w}) (shifted vertically for clarity), source-detector separation 12 mm, source-sample separation 6 mm, 0 mm sample offset from the source-detector direction. The theoretical absorption efficiency of 250 nm Au is added for comparison.

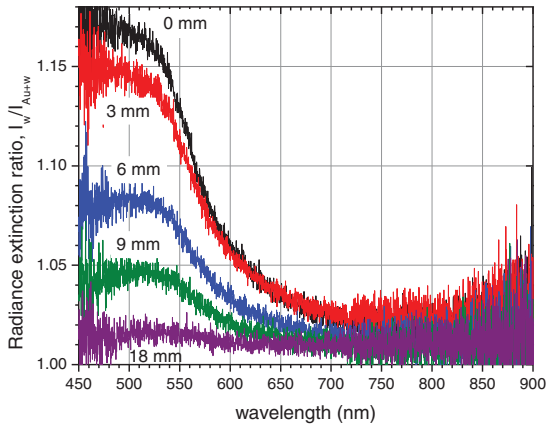

Fig. 6 Radiance extinction ratio of Au in Intralipid, (I_w/I_{Au+w}). Source-detector separation 12 mm, 0 to 18 mm sample offset from the mid-point in the source-detector direction.

known. The second feature is that the effect of water, observed as a characteristic dip at 750 nm, is removed after proper referencing to the water sample. Indeed, once the effect of water is removed, the experimentally obtained spectrum of Au NPs agrees with the calculated absorption (Fig. 5).

The results for some other offset values (with water effects removed) are shown in Fig. 6. Translation of the sample laterally introduces a change in the sample-detector separation. In Fig. 6, the first curve corresponds to a 0 mm offset and the last one to an 18 mm offset. It is evident that Au NPs can be detected at distances up to 18 mm, even when the detector is not facing the sample.

To isolate the effect of the angular position from the radial distance, the tube with Au NPs was positioned at a constant distance of 6 mm from the detector keeping 12 mm as a source-detector separation and varying the sample's angle (0, 45, 90, 135, and 180 deg) relative to the source-detector direction. A 0 deg angle corresponded to the sample position between the source and the detector (i.e., on-axis). A detailed example is provided for the Au NPs sample placed at an angle of 135 deg. White light spectroscopy offers, in principle, a continuum of wavelengths for analysis. Since plasmonic enhanced absorption dominates scattering under the experimental conditions used, a wavelength of 520 nm (close to the maximum absorption of Au NPs) was chosen for the angular polar plots. Figure 7(a) shows two raw radiance profiles: one, for Intralipid only, and the other for the Au NPs sample present in Intralipid at a 135 deg angle. Placing the sample at 135 deg lowers the collected intensity at all detector angles. However, the angular distortion of the profile due to the sample is not obvious in Fig. 7(a). Figure 7(b) shows the ratio of two profiles from part (a) that correspond to the extinction ratio I_I/I_{Au+w}, according to the previously described notation. If the sample would provide an isotropic reduction of the signal collected at all angles, the polar plot of the extinction ratio would be a circle. If the sample would provide a preferential reduction of the signal in the direction of the sample, then the ratio I_I/I_{Au+w} will show the maximum in this direction. Indeed, this type of distortion in a vicinity of 135° is seen clearly in Fig. 7(b). Water effects can be excluded from the angular profiles by analyzing I_w/I_{Au+w}. Figure 8 presents re-plotted I_w/I_{Au+w} for various angular positions of the sample on a linear x,y-scale. This representation allows better tracing of the sample location (marked by arrows) through the maxima in the profiles. Simple calculations show that a 3.5 mm diameter tube positioned at 6 mm distance from the detector will be seen in the ~30 deg window. Given an estimated accuracy in the sample positioning (~1 mm) and a 30 deg detection window, there is a good match between the targeted sample locations marked by arrows and the positions of the maxima in Fig. 8 for all angular positions, except 0 deg (not shown). The corresponding ratio for 0 deg looks almost flat with no pronounced maximum. Substitution of the fixed volume of Intralipd-1% with the equivalent volume of Au colloid between the source and the detector leads to two effects

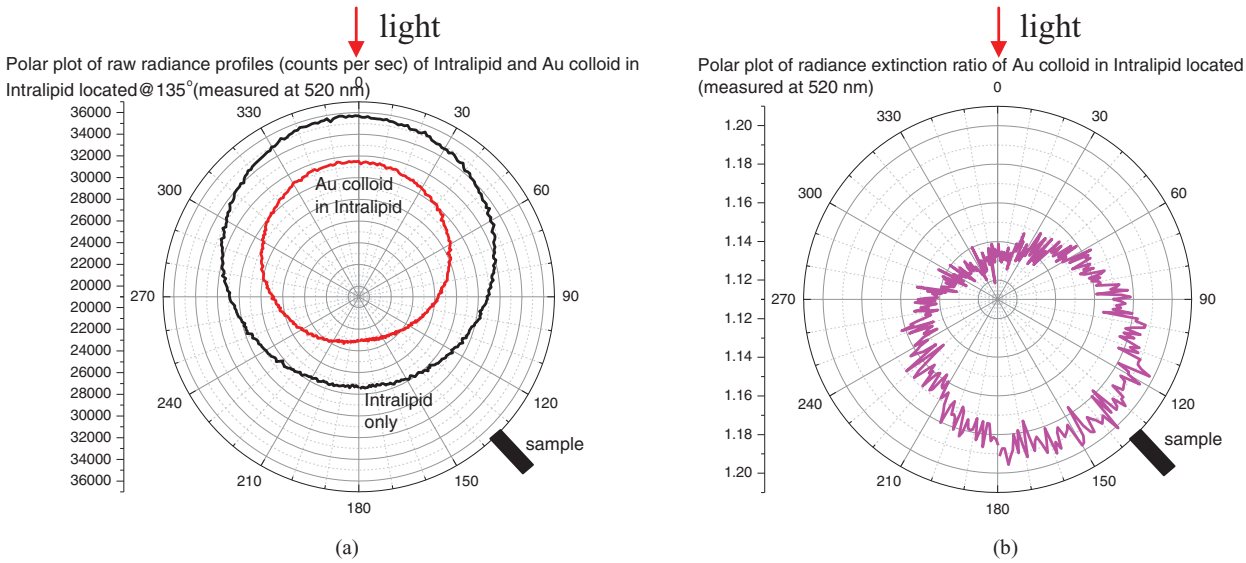

Fig. 7 (a) Polar plots of raw radiance profiles of Intralipid-1% alone and Au colloid in Intralipid-1% located at 135 deg (measured at 520 nm), (b) polar plot of radiance extinction ratio of Au colloid in Intralipid-1% (I_I/I_{Au+w}) [i.e., the ratio of the two profiles shown in (a)]. Angular position of the sample is denoted as a box.

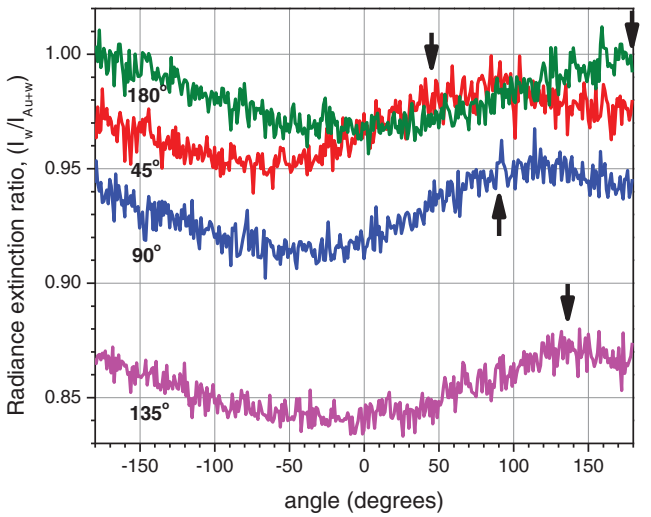

Fig. 8 Radiance extinction ratio versus detection angle at 520 nm for different sample positions (shown by an arrow).

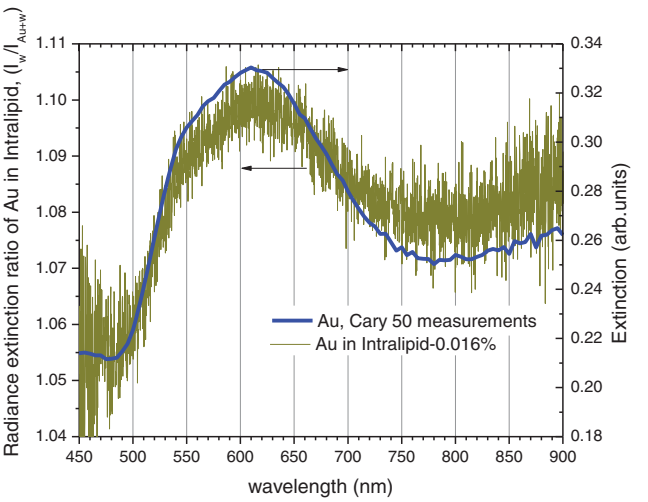

Fig. 9 Radiance extinction ratio of Au in Intralipid-0.016% and the measured (Cary 50) extinction for 250 nm Au colloid.

acting in opposite directions. Acting as a localized inclusion, water as opposed to Intralid, significantly reduces the scattering coefficient that increases the number of photons reaching the detector. Au NPs, on the other hand, increase the absorption coefficient acting as a sink for impinging photons and removing them from the subsequent diffusion process. As a result, it leads to the decrease in the signal collected by the detector. When both effects are almost of the same order, the sample is not detected in the Intralipid background. When the volume of water is reduced (via decreasing the diameter of the tube, for example) or absorption of Au NPs is increased, the profile of the radiance ratio at 0 deg will show the maximum as well. This was confirmed by performing similar experiments with 5-nm Au colloid that has an absorption coefficient higher than 250-nm Au colloid. The increase in the absorption coefficient came from a five-order increase in the particle density of the stock solution of 5-nm Au colloid, while the absorption efficiency of an individual particle dropped by a factor of ~5 compared with a 250-nm Au colloid. Overall, experiments with 5-nm Au NPs reproduce qualitatively all major results observed for 250-nm Au NPs.

An analysis of curves from Fig. 8 reveals that a difference between "on-sample" value and "off-sample" value (corresponding to the maximum and the minimum on the curves) is quite consistent for all angles: 0.03 (45 deg), 0.04 (90 deg), 0.03 (135 deg), and 0.035 (180 deg). It indicates that a contrast value of 250-nm Au NPs with a density of 3.6×10^8 particles/mL in Intralipid-1% is about 3% to 4% and does not depend on the observation angle. However, more investigations in this direction are required.

Figure 9 presents the radiance extinction ratio of 250-nm Au NPs in the solution of Intralipid diluted down to 0.016% and the optical extinction measured for the colloidal solution with a standard spectrometer (Cary 50). We performed dilutions of Intralipid-1% to confirm the "masking" effect of Intralipid on scattering of Au NPs. The source-detector separation was kept constant at 12 mm, and the sample was positioned mid-way between the source and the detector. As expected, at a certain concentration of the background medium (Intralipid-0.016%), we were able to recover the extinction spectrum of Au NP (Fig. 9) as was seen in Fig. 3, i.e., with both scattering and absorption contributing to the overall extinction. A decrease of the Intralipid concentration reduces the particle density that contributes to the value of the scattering coefficient. Taking the previously obtained value of 64 cm^{-1} for the scattering coefficient of Intralipid-1%, the scattering coefficient of Intralipid-0.016% is estimated to be ~1.0 cm^{-1} at 500 nm. It starts to approach the one of the Au NPs (i.e., ~ 0.75 cm^{-1}). This simple estimation supports the transition observed at the specific concentration. It has important implications for using Au NPs as contrast agents in scattering-based optical techniques. Due to the interplay between scattering coefficients of the background tissue and Au NPs, scattering signatures of individual Au NPs may be lost. The total scattering can be dominated by the background tissue scattering, and hence, the image contrast may be limited. It is understood, however, that this effect depends not only on a simple ratio of scattering coefficients of the background and the chromophore of interest, but on the effective optical thickness of the background. This has applications both for deep tissue imaging and confocal optical microscopy in highly scattering tissues. Because of the diffused light propagation regime, a complex geometrical/statistical model needs to be scrutinized thoroughly to estimate the value of the effective optical thickness. It is important to note that Au NPs with plasmon resonance in the visible range were used in this proof of principle investigation. It is understood that biological tissues would require nanoparticles with resonances in the biomedical transparency window (i.e., ~650 to ~1000 nm).

When translated to biological tissues, the approach is contingent on the ability to perform proper reference measurements in order to detect relative changes in tissue optical properties caused by any external treatment. In the context of the article, relative changes are brought by introducing localized exogenous chromophores (i.e., Au nanoparticles) as specific markers for diagnostic or treatment purposes. Considering prostate as a potential target and the two-fiber approach developed in the paper, we envisage the following methodology. An optical source fiber is inserted into the rectum and the detecting fiber into the urethra. Both fibers will be accommodated via specially

designed catheters. The insertion depth of both fibers should be controlled. Once the desired targeted depth is reached, axial translation of both fibers with subsequent angular radiance acquisition measurements can offer potential 3D optical mapping. A baseline radiance profile would be obtained prior to any intervention. Systemically delivered and functionalized Au NPs with specific binding to tumor sites or nonfunctionalized Au NPs with preferential accumulation at tumor sites (due to the enhanced permeability and retention effect) will yield a perturbation in the radiance profile. The ratio approach described in the paper will be used for analysis. Additional studies are required to determine how the spatial extent of the perturbation would affect lower and upper limits of detection. Moreover, the maximum detection distance will depend on the optical attenuation of the prostate. To provide adequate illumination within the entire prostate (~5 cm), more intense white light sources with output powers of several hundred milliwatts may be required.

To preserve the angular resolution, the detected signal must be radiance and not fluence. If the functionalities of the two fibers in the set-up are switched (i.e., illumination through the side firing fiber with rotation and detection via the isotropic spherical diffuser), multiple scattering will randomize photon pathways providing a nonselective isotropic illumination pattern. Therefore, the detected fluence will lose the specificity of the source-target interaction and therefore, the spatial content. However, a combination of two side firing fibers (used interchangeably as the source and the detector) may have some interesting properties by providing the absolute spatial coordinate in addition to the angle of the localized inhomogeneity based on simple geometrical considerations.

4 Conclusions

We have developed a versatile technique based on point radiance spectroscopy for studying light propagation inside liquid biological phantoms. Deep-tissue white-light spectroscopy provides spectral identification of Au NPs acting as chromophores of interest. When Au NPs possessing both scattering and absorption are used as localized exogenous chromophores in Intralipid-1% background, the Intralipid scattering prevents the detection of plasmon scattering such that plasmon absorption remains the only detectable optical signature. The results demonstrate that the presence of Au NPs in the turbid medium introduces changes in the radiance extinction ratio over an entire 360 deg range. The chromophore manifests a prominent feature in the direction of its location, i.e., the maximum in the radiance extinction ratio that allows its unambiguous angular localization inside turbid media. We have demonstrated a feasibility of using point radiance spectroscopy as a minimally invasive modality for prostate imaging with Au NPs as contrast agents.

Acknowledgments

The authors thank Dr. Bruce Brinson (Rice University) for providing Mie theory calculations. The authors acknowledge financial support from NSERC, CIHR, AIF, and Canada Research Chair program (W. M. Whelan).

References

1. R. Chapman, "New therapeutic technique for treatment of uterine leiomyomas using laser-induced interstitial thermotherapy (LITT) by a minimally invasive method," *Lasers Surg. Med.* **22**(3), 171–178 (1998).
2. H. Atsumi, M. Matsumae, M. Kaneda, I. Muro, Y. Mamata, T. Komiya, A. Tsugu, and R. Tsugane, "Novel laser system and laser irradiation method reduced the risk of carbonization during laser interstitial thermotherapy: assessed by MR temperature measurement," *Lasers Surg. Med.* **29**(2), 108–117 (2001).
3. T. J. Vogl, R. Straub, S. Zangos, M. G. Mack, and K. Eichler, "MR-guided laser-induced thermotherapy (LITT) of liver tumours: experimental and clinical data," *Int. J. Hyperthermia* **20**(7), 713–724 (2004).
4. T. C. Zhu, J. C. Finlay, and S. M. Hahn, "Determination of the distribution of light, optical properties, drug concentration, and tissue oxygenation in vivo in human prostate during motexafin lutetium-mediated photodynamic therapy," *J. Photochem. Photobiol. B* **79**(3), 231–241 (2005).
5. G. Zaccanti, S. Del Bianco, and F. Martelli, "Measurements of optical properties of high-density media," *App. Opt.* **42**(19), 4023–4030 (2003).
6. A. Dimofte, J. C. Finlay, and T. C. Zhu, "A method for determination of the absorption and scattering properties interstitially in turbid media," *Phys. Med. Biol.* **50**(10), 2291–2311 (2005).
7. D. J. Dickey, R. B. Moore, D. C. Rayner, and J. Tulip, "Light dosimetry using the P3 approximation," *Phys. Med. Biol.* **46**(9), 2359–2370 (2001).
8. L. C. L. Chin, W. M. Whelan, and I. A. Vitkin, "Information content of point radiance measurements in turbid media: implications for interstitial optical property quantification," *Appl. Optics* **45**(9), 2101–2114 (2006).
9. L. C. L. Chin, B. Lloyd, W. M. Whelan, and I. A. Vitkin, "Interstitial point radiance spectroscopy of turbid media," *J. Appl. Phys.* **105**(10), 102025 (2009).
10. P. K. Jain, K. S. Lee, I. H. El-Sayed, and M. A. El-Sayed, "Calculated absorption and scattering properties of gold nanoparticles of different size, shape, and composition: applications in biological imaging and biomedicine," *J. Phys. Chem. B* **110**(14), 7238–7248 (2006).
11. C. F. Bohren and D. R. Huffman, *Absorption and Scattering of Light by Small Particles*, Wiley-VCH, Weinheim (2004).
12. C. Loo, L. Hirsch, M.-H. Lee, E. Chang, J. West, N. Halas, and R. Drezek, "Gold nanoshell bioconjugates for molecular imaging in living cells," *Opt. Lett.* **30**(9), 1012–1014 (2005).
13. P. Puvanakrishnan, J. Park, P. Diagaradjane, J. A. Schwartz, C. L. Coleman, K. L. Gill-Sharp, K. L. Sang, J. D. Payne, S. Krishnan, and J. W. Tunnel, "Near-infrared narrow-band imaging of gold/silica nanoshells in tumors," *J. Biomed. Opt.* **14**(2), 024044 (2009).
14. L. R. Hirsch, R. J. Stafford, J. A. Bankson, S. R. Sershen, B. Rivera, R. E. Price, J. D. Hazle, N. J. Halas, and J. L. West, "Nanoshell mediated near-infrared thermal therapy of tumors under magnetic resonance guidance," *Proc. Natl. Acad. Sci. U.S.A.* **100**(23), 13549–13554 (2003).
15. S. Krishnan, P. Diagaradjane, and S. H. Cho, "Nanoparticle-mediated thermal therapy: evolving strategies for prostate cancer therapy," *Int. J. Hyperthermia* **26**(8), 775–789 (2010).
16. N. N. Boustany, S. A. Boppart, and V. Backman, "Microscopic imaging and spectroscopy with scattered light," *Annu. Rev. Biomed. Eng.* **12**, 285–314 (2010).
17. A. L. Oldenburg, M. N. Hansen, D. A. Zweifel, A. Wei, and S. Boppart, "Plasmon-resonant gold nanorods as low backscattering albedo contrast agents for optical coherence tomography," *Opt. Express* **14**(15), 6724–6738 (2006).
18. A. W. H. Lin, N. A. Lewinski, M. H. Lee, and R. A. Drezek, "Reflectance spectroscopy of gold nanoshells: computational predications and experimental measurements," *J. Nanopart. Research* **8**(5), 681–692 (2006).
19. R. Michels, F. Foschum, and A. Kienle, "Optical properties of fat emulsions," *Opt. Express* **16**(8), 5907–5925 (2008).
20. V. A. McGlone, P. Martinsen, R. Kunnemeyer, B. Jordan, and B. Cletus, "Measuring optical temperature coefficients of Intralipid," *Phys. Med. Biol.* **52**(9), 2367–2378 (2007).
21. J. S. Dam, C. B. Pedersen, T. Dalgaard, P. E. Fabricius, P. Aruna, and S. Anderson-Engels, "Fiber-optic probe for noninvasive real-time determination of tissue optical properties at multiple wavelengths," *Appl. Optics* **40**(7), 1155–1164 (2001).

22. M. Solonenko, R. Cheung, T. M. Busch, A. Kachur, G. M. Griffin, T. Vulcan, T. C. Zhu, H. W. Wang, S. M. Hahn, and A. G. Yodh, "In vivo reflectance measurements of optical properties, blood oxygenation, and motexafin lutetium uptake in canine large bowels, kidneys and prostate," *Phys. Med. Biol.* **47**(6), 857–873 (2002).
23. Based on the BHMIE algorithm for the homogenous sphere published in appendix the book of C. F. Bohren and D. R. Huffman, *Absorption and Scattering of Light by Small Particles*, Wiley-VCH, Weinheim (2004).
24. D. K. Mynbaev and L. L Scheiner, Chap. 3, in *Fiber-Optic Communications Technology*, Prentice Hall, New Jersey (2001).
25. C. F. P. van Swol, R. M. Verdaasdonk, R. J. van Vliet, D. G. Molenaar, and T. A. Boon, "Side-firing devices for laser prostatectomy," *World J. Urol.* **13**(2), 88–93 (1995).
26. O. Barajas, A. M. Ballangrud, G. G. Miller, R. B. Moore, and J. Tulip, "Monte Carlo modeling of angular radiance in tissue phantoms and human prostate: PDT light dosimetry," *Phys. Med. Biol.* **42**(9), 1675–1687 (1997).
27. T. Xu, C. P Zhang, G. Y Chen, J. G Tian, G. Y Zhang, and C. M. Zhao, "Theoretical and experimental study of the intensity distribution in biological tissues," *Chin. Phys.* **14**(9), 1813–1820 (2005).